Supplementary Materials Document 2: Original Figures Not Shown in the Edited Paper

Samvel S. Grigorian and Alexander V. Ostroumov

Figure captions compiled by Dieter Issler

November 15, 2019

This document contains all plots from the appendix to the original manuscript that were not inserted into the edited version of the paper for the sake of conciseness.

The original manuscript does not contain figure captions. To facilitate reading, the editor added the most relevant information as inferred from the text.

The parameter values used in the simulations related to Figures S2.1–S2.9 are listed in Table 4.1 of the edited paper.

Note that some of the plots (Figures S2.9.a, S2.10.c and d, S2.11) display the limit frictional shear stress, τ_*, or the strength parameter of the snow cover, p_*, in the gravitational metric system, i.e., in terms of τ_*/g or p_*/g and thus in units of $\mathrm{kg\,m^{-2}}$. In the conversion to standard SI units of Pa, $g \approx 10\,\mathrm{m\,s^{-2}}$ was applied.

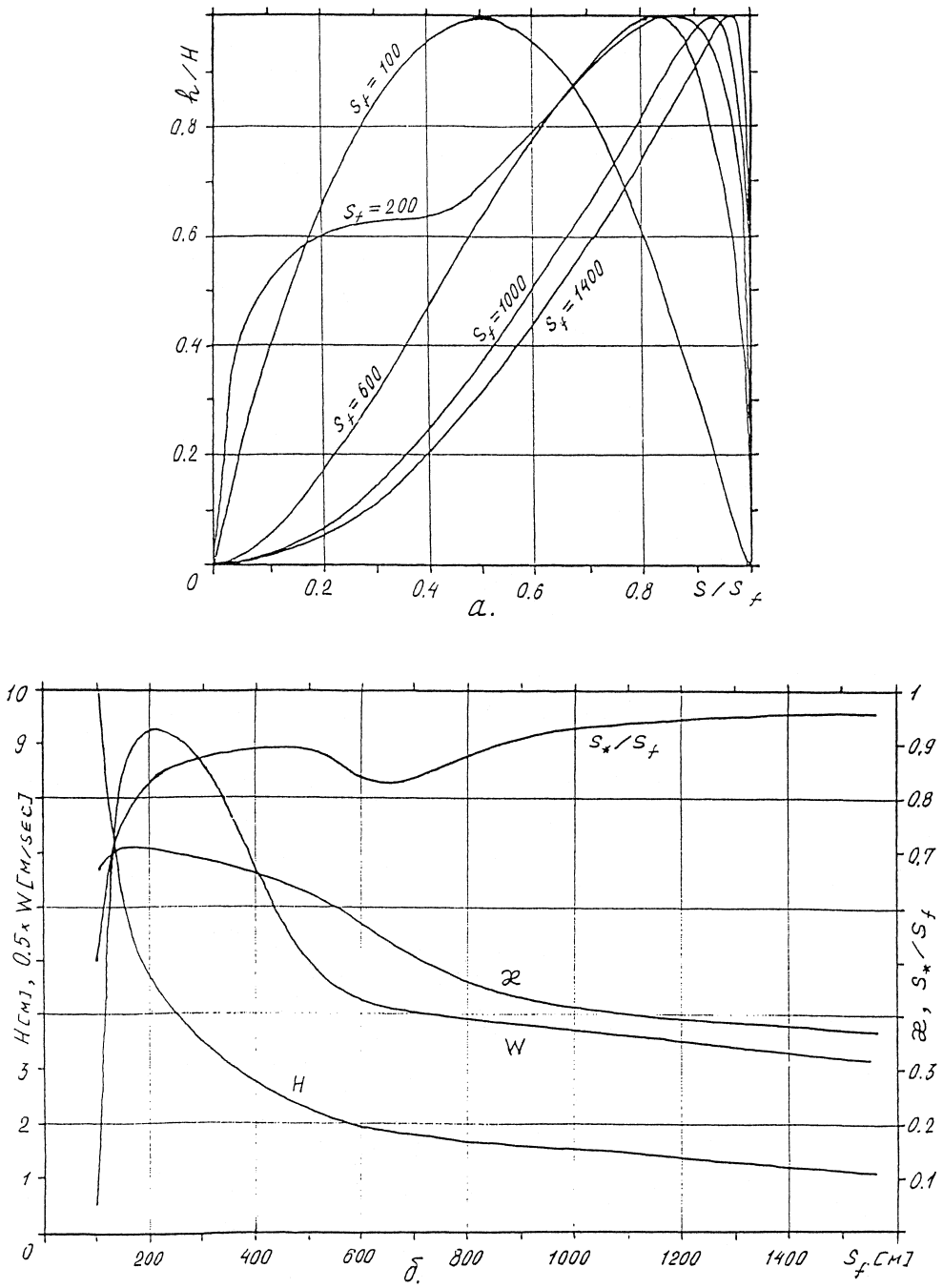

Figure S2.1: Numerical results from simulations with the full model, variant 2. The initial velocity is reduced from $10\,\mathrm{m\,s^{-1}}$ to $1\,\mathrm{m\,s^{-1}}$, and the maximum release depth increased from 1 m to 10 m. (**a**) Selected longitudinal profiles of h/H (the flow depth h scaled by the instantaneous maximum flow depth H) as a function of S/S_f, the position relative to the instantaneous front position. (**b**) Evolution of the front velocity w (left-hand scale, in units of $2\,\mathrm{m\,s^{-1}}$), the maximum flow depth H (left-hand scale, in m), the relative position of the maximum flow depth, S_*/S_f (right-hand scale), and the shape factor $\varkappa$ (right-hand scale), with front position S_f.

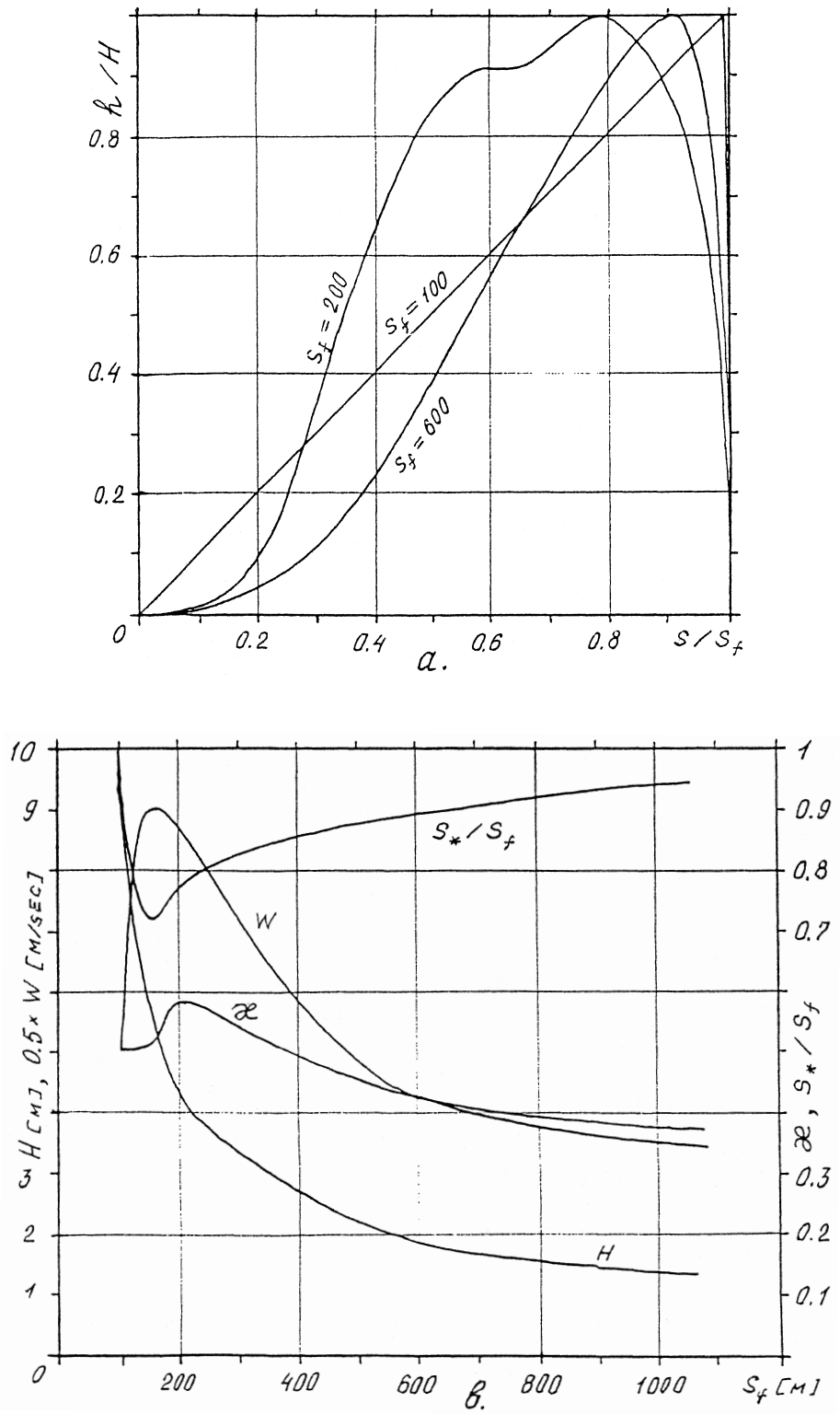

Figure S2.2: Numerical results from simulations with the full model, variant 3. The parabolic shape of the release mass in the base configurations is replaced by a triangular shape of height 10 m in this simulation. (**a**) Evolution of the longitudinal profile of the flow depth h, scaled by the instantaneous front positions S_f (in m), and maximum depth, $H(S_f)$, of the flow. (**b**) Evolution of the front velocity w (left-hand scale, in units of $2\,\mathrm{m\,s^{-1}}$), the maximum flow depth H (left-hand scale, in m), the relative position of the maximum flow depth, S_*/S_f (right-hand scale), and the shape factor $\varkappa$ (right-hand scale), with front position S_f.

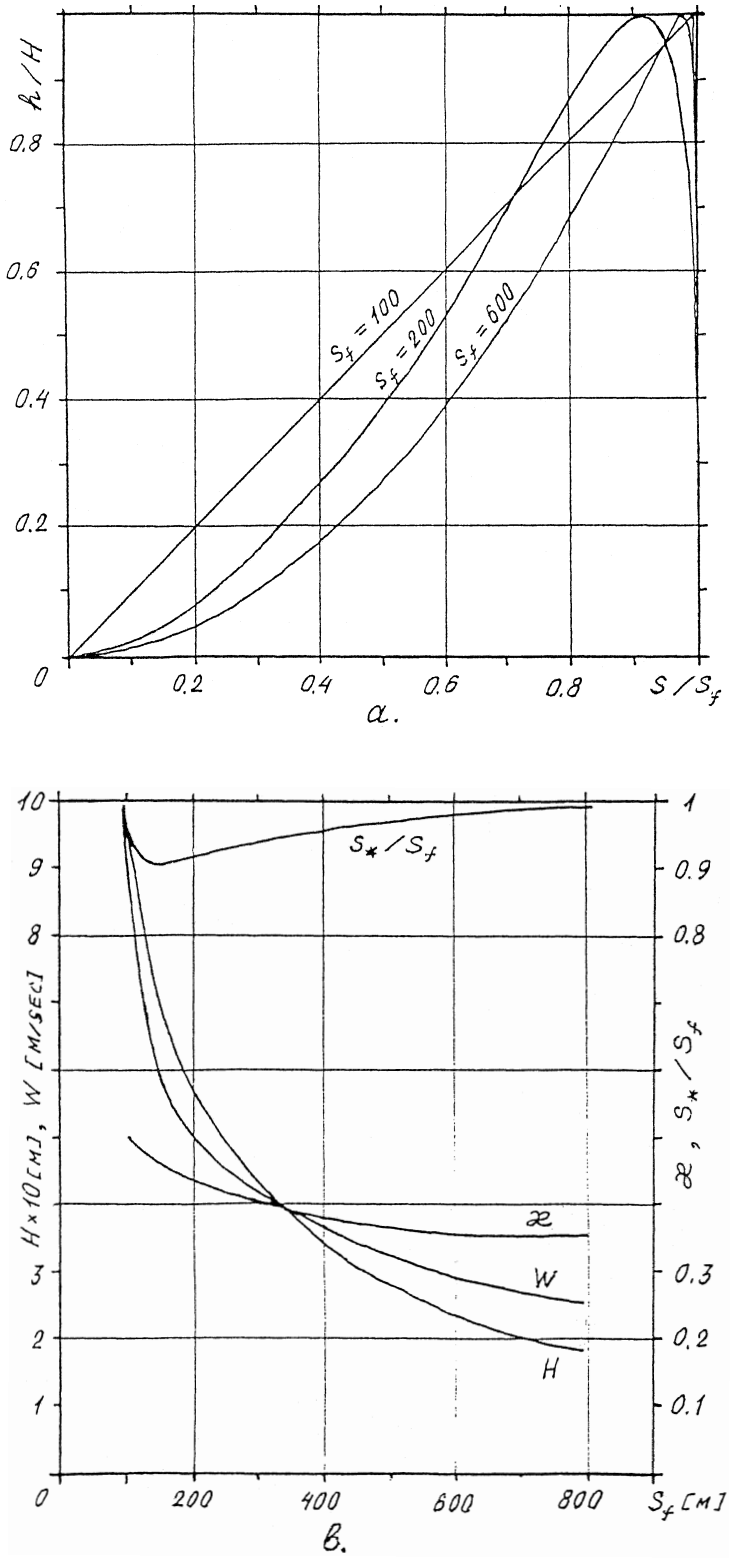

Figure S2.3: Numerical results from simulations with the full model, variant 4. The parabolic shape of the release mass in the base configurations is replaced by a triangular shape of height 1 m in this simulation. (**a**) Selected longitudinal profiles of h/H (the flow depth h scaled by the instantaneous maximum flow depth H) as a function of S/S_f, the position relative to the instantaneous front position. (**b**) Evolution of the front velocity w (left-hand scale, in units of $\mathrm{m\,s^{-1}}$), the maximum flow depth H (left-hand scale, in m), the relative position of the maximum flow depth, S_*/S_f (right-hand scale), and the shape factor $\varkappa$ (right-hand scale), with front position S_f.

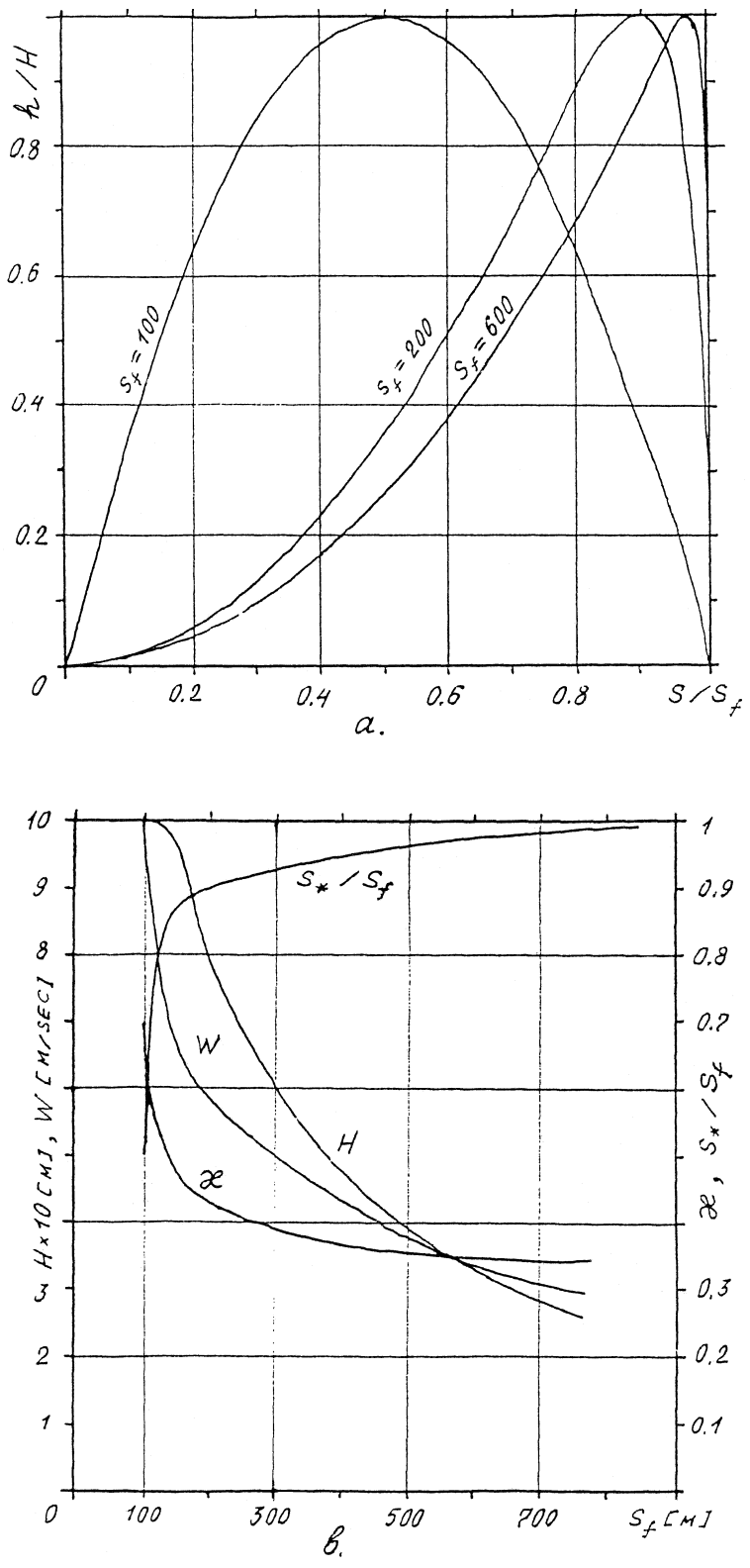

Figure S2.4: Numerical results from simulations with the full model, variant 5. (**a**) Selected longitudinal profiles of h/H (the flow depth h scaled by the instantaneous maximum flow depth H) as a function of S/S_f, the position relative to the instantaneous front position. (**b**) Evolution of the front velocity w (left-hand scale, in units of $\mathrm{m\,s^{-1}}$), the maximum flow depth H (left-hand scale, in m), the relative position of the maximum flow depth, S_*/S_f (right-hand scale), and the shape factor $\varkappa$ (right-hand scale), with front position S_f.

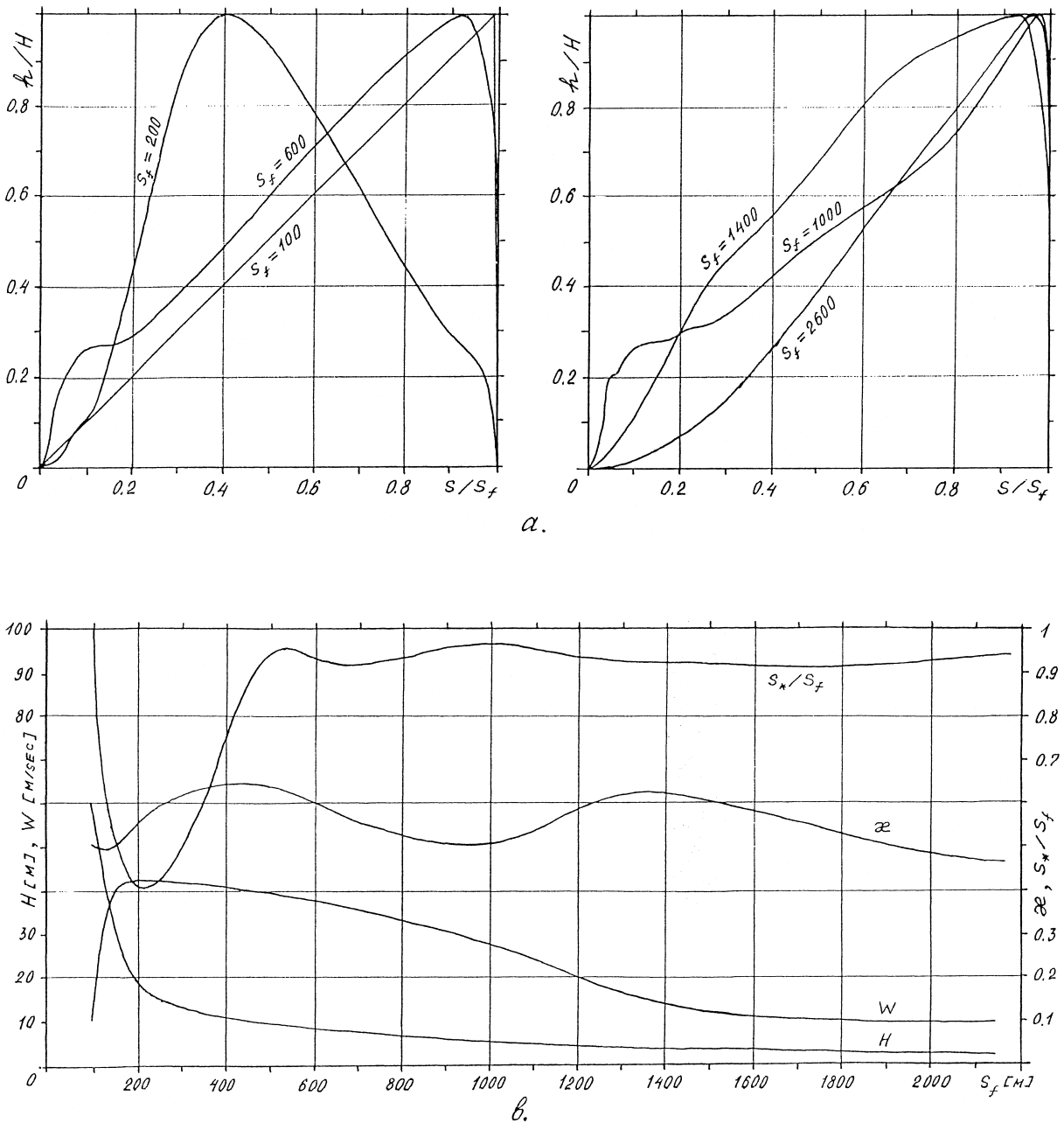

Figure S2.5: Numerical results from simulations with the full model, variant 6. Here, the release mass has the shape of a triangle with height 60 m. (**a**) Selected longitudinal profiles of h/H (the flow depth h scaled by the instantaneous maximum flow depth H) as a function of S/S_f, the position relative to the instantaneous front position. (**b**) Evolution of the front velocity w (left-hand scale, in units of $\mathrm{m\,s^{-1}}$), the maximum flow depth H (left-hand scale, in m), the relative position of the maximum flow depth, S_*/S_f (right-hand scale), and the shape factor $\varkappa$ (right-hand scale), with front position S_f.

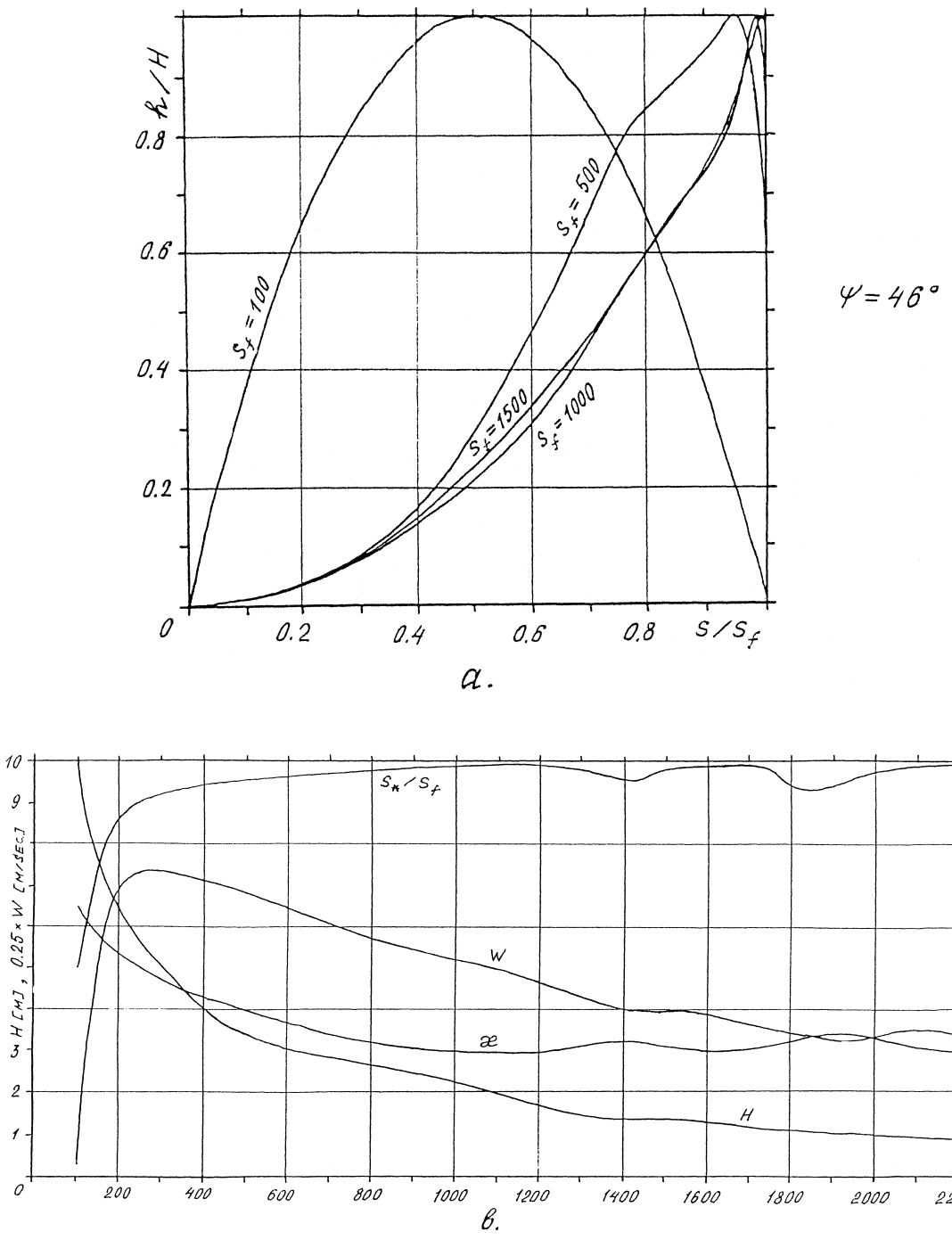

Figure S2.6: Numerical results from simulations with the full model, variant 7. The slope angle is set to 46°, the initial velocity to $1\,\mathrm{m\,s^{-1}}$, and the maximum release depth to 10 m. (**a**) Selected longitudinal profiles of h/H (the flow depth h scaled by the instantaneous maximum flow depth H) as a function of S/S_f, the position relative to the instantaneous front position. (**b**) Evolution of the front velocity w (left-hand scale, in units of $4\,\mathrm{m\,s^{-1}}$), the maximum flow depth H (left-hand scale, in m), the relative position of the maximum flow depth, S_*/S_f (right-hand scale), and the shape factor $\varkappa$ (right-hand scale), with front position S_f.

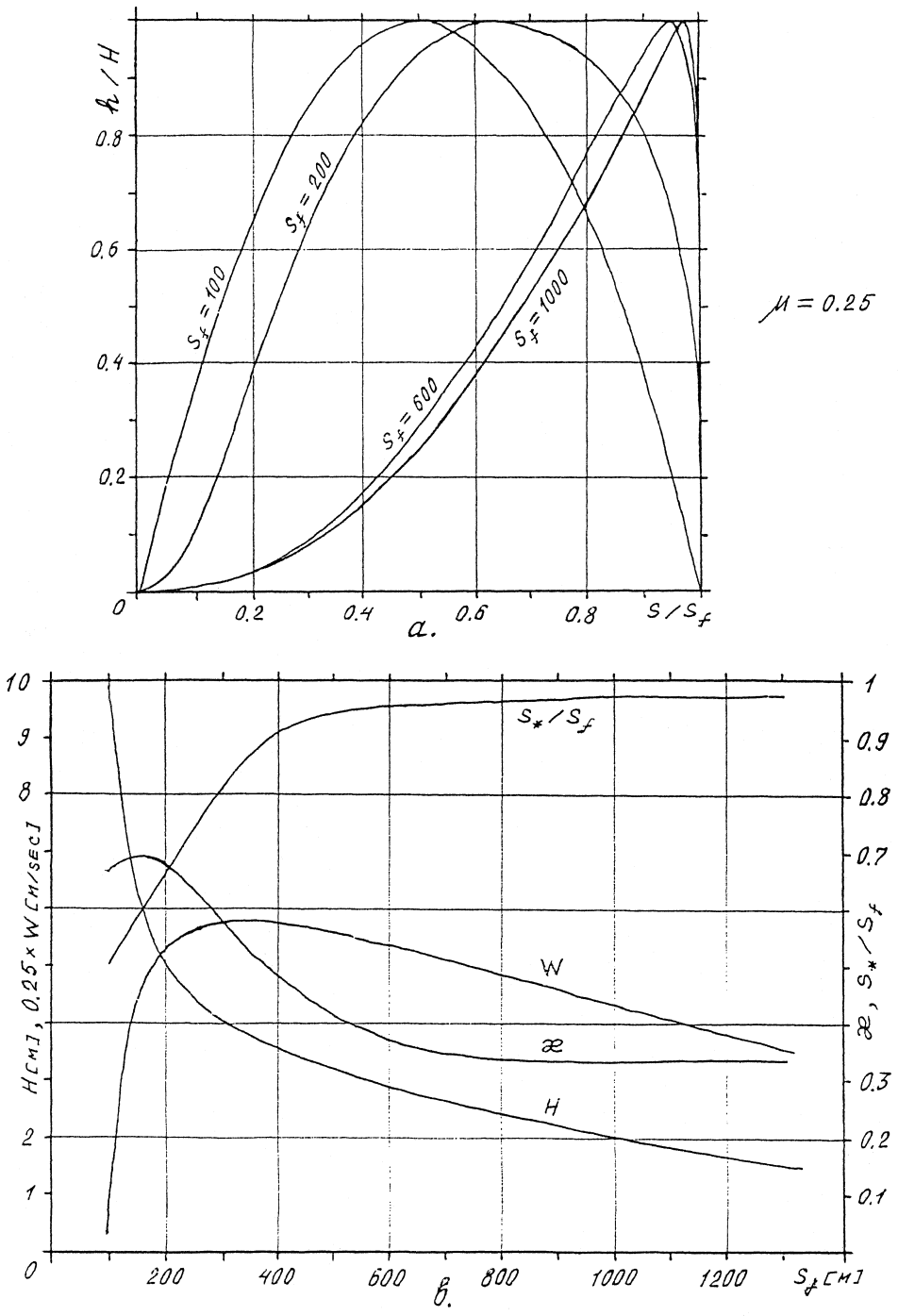

Figure S2.7: Numerical results from simulations with the full model, variant 8 (dry-friction coefficient μ set to 0.25 instead of 0.5). (**a**) Selected longitudinal profiles of h/H (the flow depth h scaled by the instantaneous maximum flow depth H) as a function of S/S_f, the position relative to the instantaneous front position. (**b**) Evolution of the front velocity w (left-hand scale, in units of $4\,\mathrm{m\,s^{-1}}$), the maximum flow depth H (left-hand scale, in m), the relative position of the maximum flow depth, S_*/S_f (right-hand scale), and the shape factor $\varkappa$ (right-hand scale), with front position S_f.

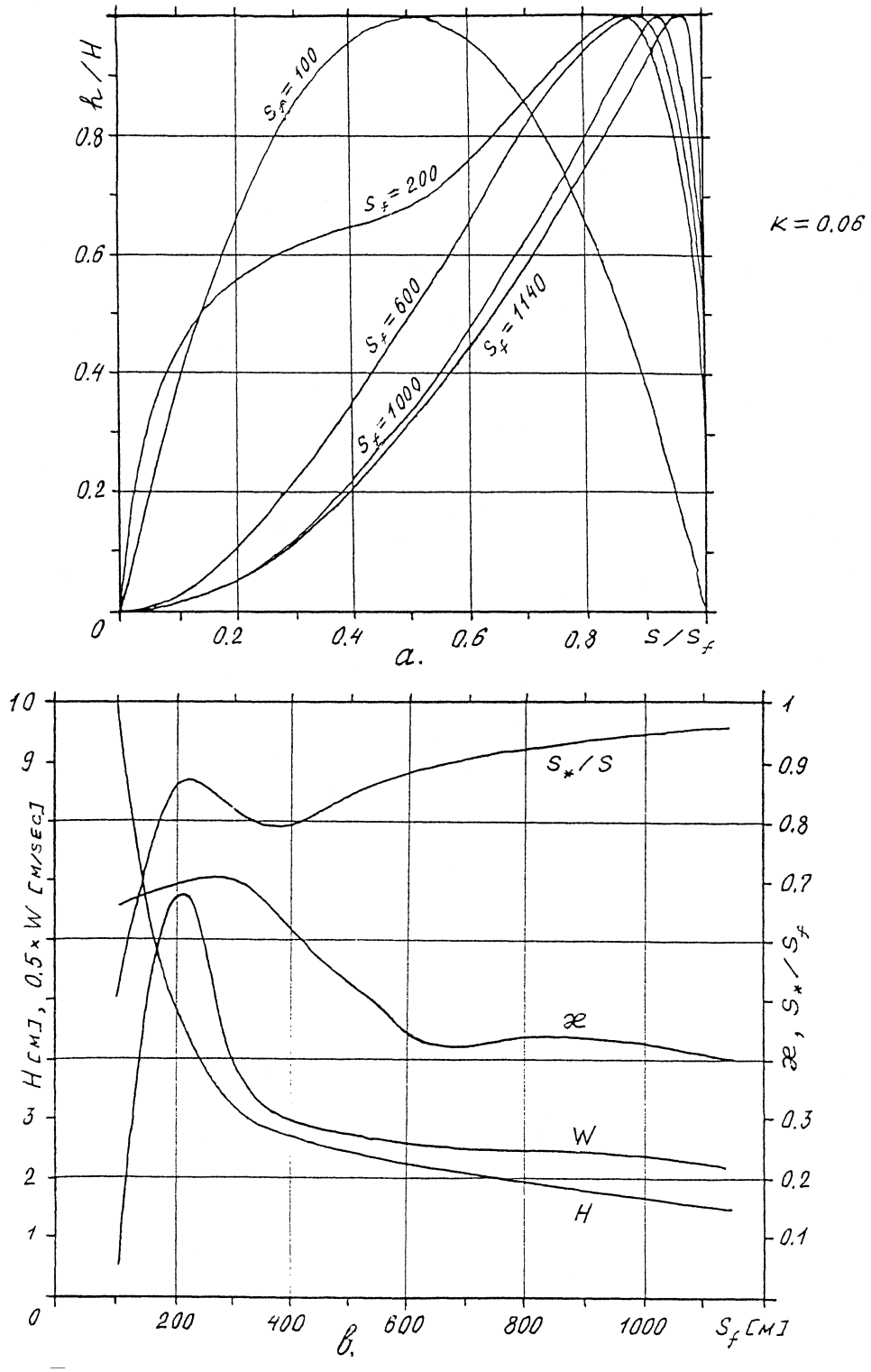

Figure S2.8: Numerical results from simulations with the full model, variant 9. The drag coefficient k is set to 0.06 instead of 0.02. (**a**) Selected longitudinal profiles of h/H (the flow depth h scaled by the instantaneous maximum flow depth H) as a function of S/S_f, the position relative to the instantaneous front position. (**b**) Evolution of the front velocity w (left-hand scale, in units of $2\,\mathrm{m\,s^{-1}}$), the maximum flow depth H (left-hand scale, in m), the relative position of the maximum flow depth, S_*/S_f (right-hand scale), and the shape factor $\varkappa$ (right-hand scale), with front position S_f.

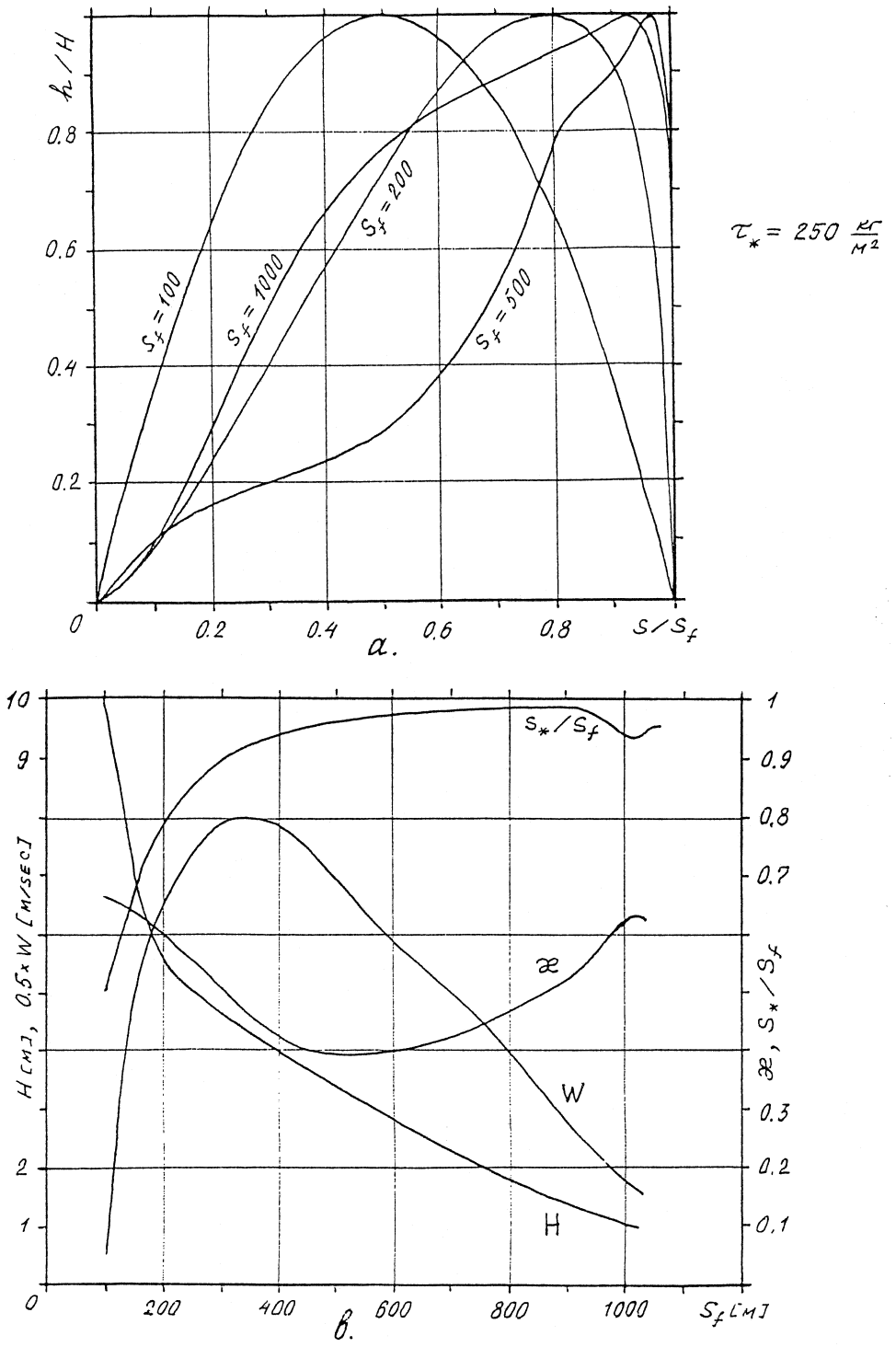

Figure S2.9: Numerical results from simulations with the full model, variant 10 (maximum shear stress set to 2.5 kPa instead of 10 kPa). (**a**) Selected longitudinal profiles of h/H (the flow depth h scaled by the instantaneous maximum flow depth H) as a function of S/S_f, the position relative to the instantaneous front position. (**b**) Evolution of the front velocity w (left-hand scale, in units of $2\,\mathrm{m\,s^{-1}}$), the maximum flow depth H (left-hand scale, in m), the relative position of the maximum flow depth, S_*/S_f (right-hand scale), and the shape factor $\varkappa$ (right-hand scale), with front position S_f.

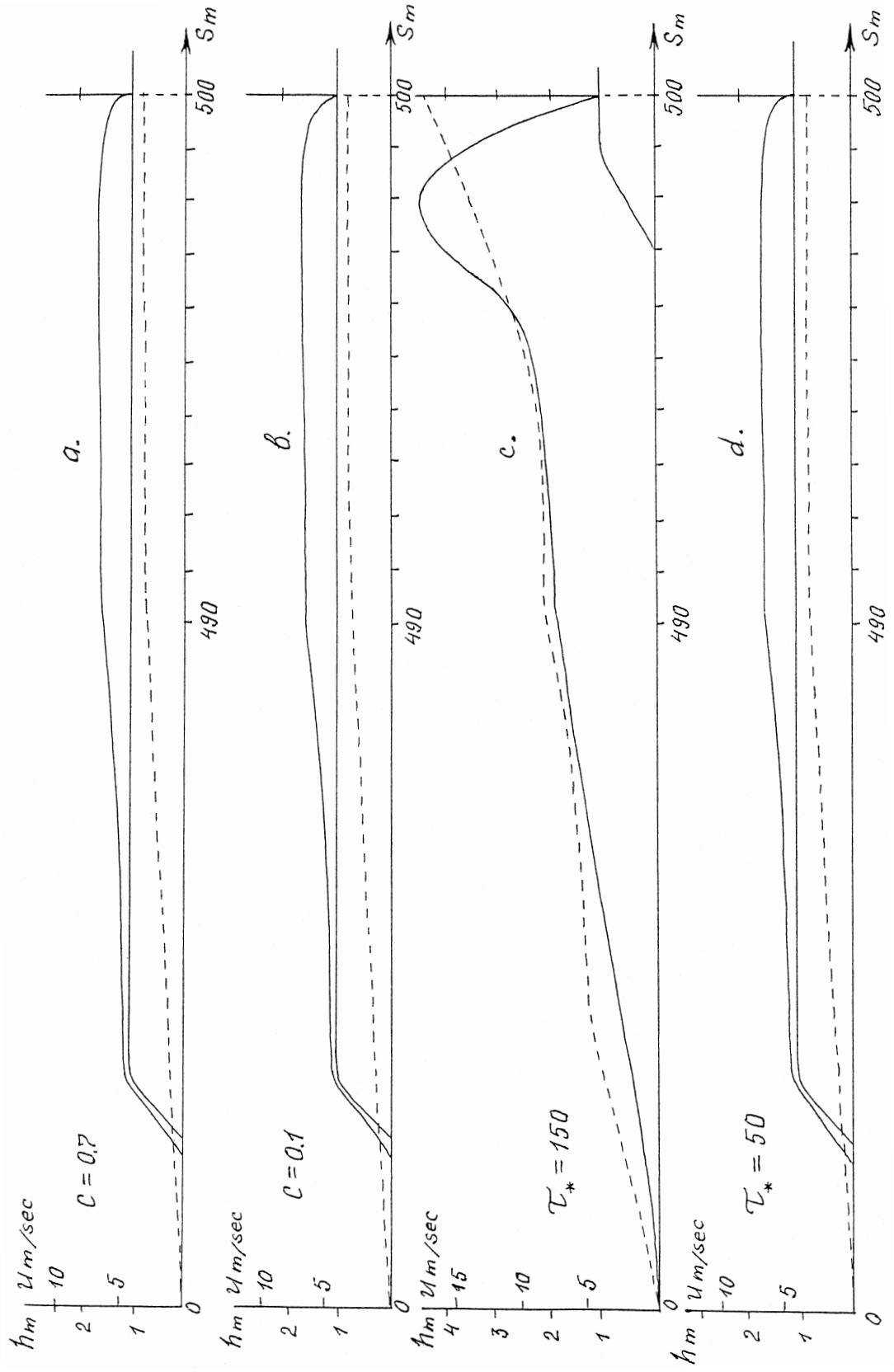

Figure S2.10: Numerical results from simulations with the full model. Note the change of horizontal scale at $S = 490\,\mathrm{m}$. In each plot, the modified parameter values relative to the standard set $\mu = 0.25$, $k = 0.1$, $\tau_* = p_* = 4\,\mathrm{kPa}$, $C = \sigma = 1$, $\rho = \rho_0 = 300\,\mathrm{kg\,m^{-3}}$ are indicated (values of τ_* are shown in units of $10\,\mathrm{Pa}$).

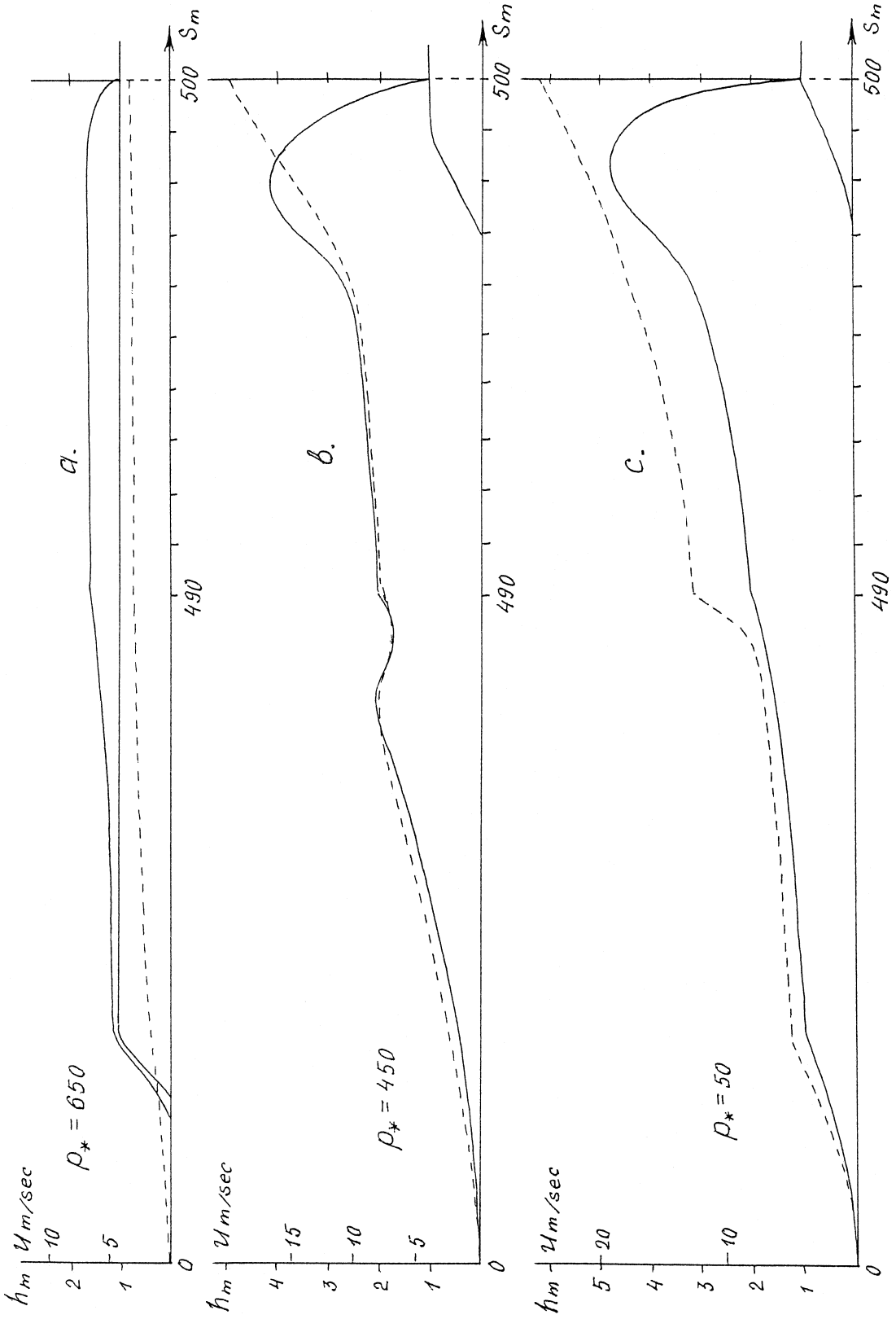

Figure S2.11: Numerical results from simulations with the full model. Note the change of horizontal scale at $S = 490\,\mathrm{m}$. In each plot, the modified parameter values relative to the standard set $\mu = 0.25$, $k = 0.1$, $\tau_* = p_* = 4\,\mathrm{kPa}$, $C = \sigma = 1$, $\rho = \rho_0 = 300\,\mathrm{kg\,m^{-3}}$ are indicated (values of p_* are shown in units of $0.1\,\mathrm{Pa}$).

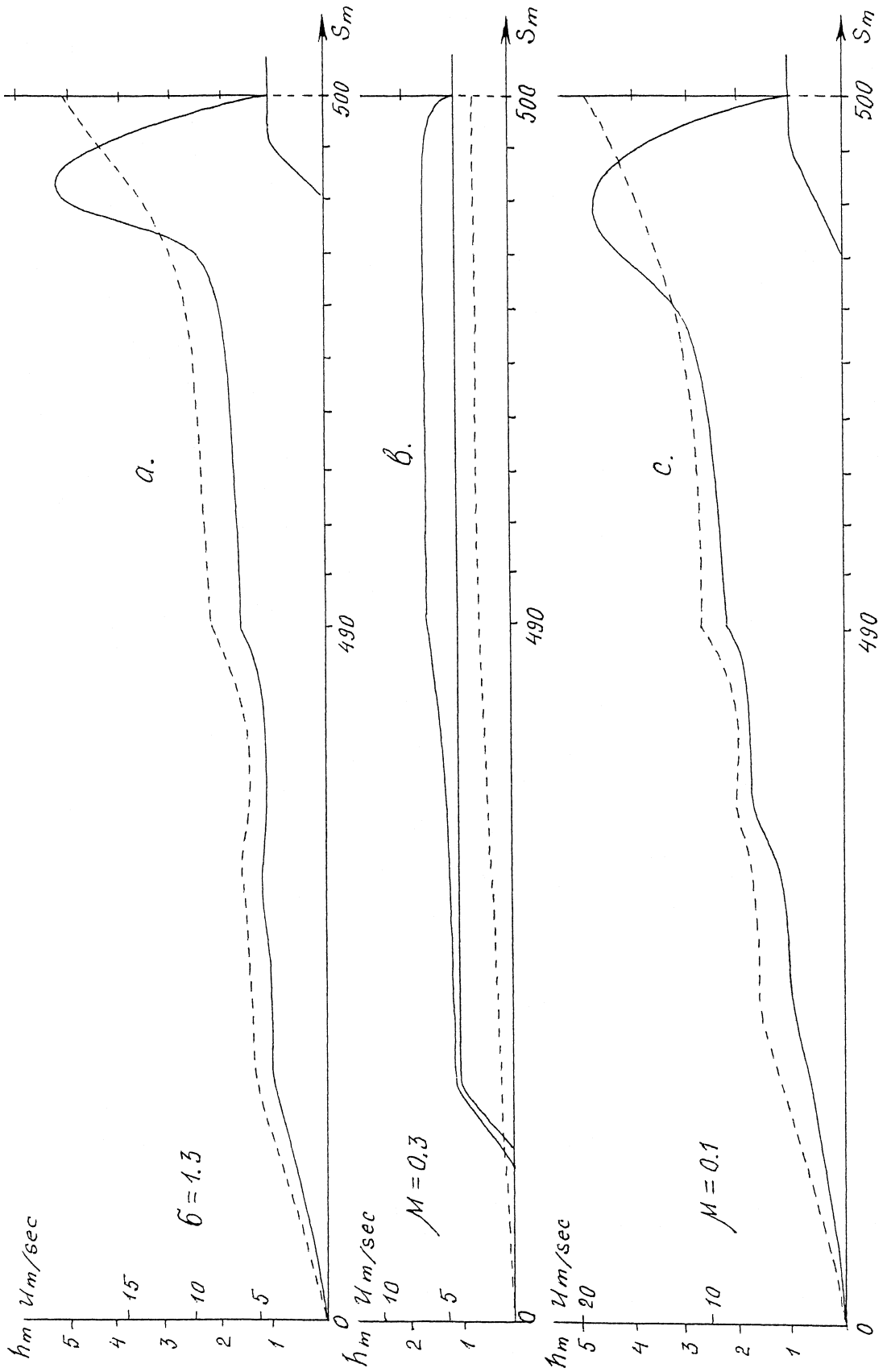

Figure S2.12: Numerical results from simulations with the full model. Note the change of horizontal scale at $S = 490\,\mathrm{m}$. In each plot, the modified parameter values relative to the standard set $\mu = 0.25$, $k = 0.1$, $\tau_* = p_* = 4\,\mathrm{kPa}$, $C = \sigma = 1$, $\rho = \rho_0 = 300\,\mathrm{kg\,m^{-3}}$ are indicated.

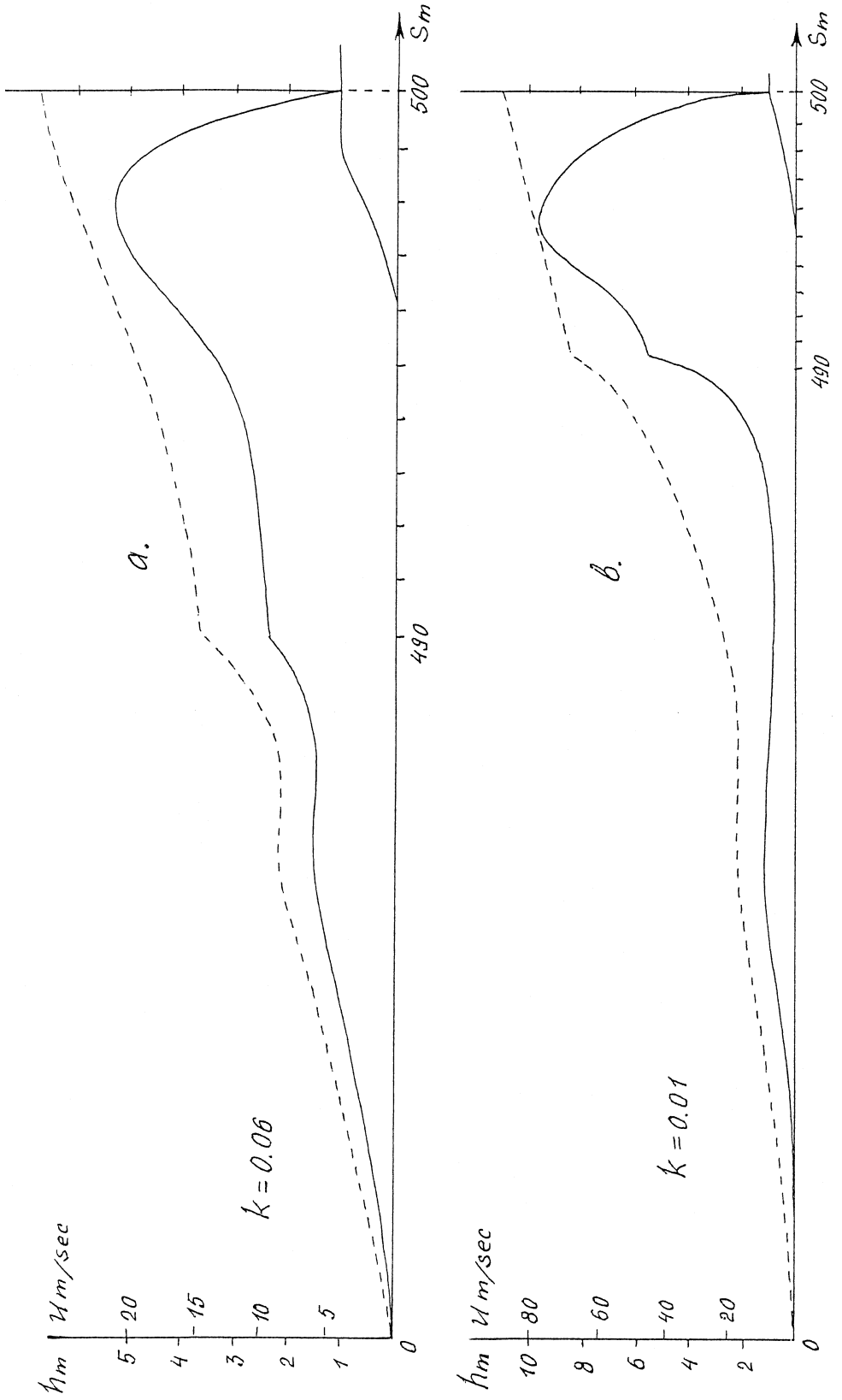

Figure S2.13: Numerical results from simulations with the full model. Note the change of horizontal scale at $S = 490\,\mathrm{m}$. In each plot, the modified parameter values relative to the standard set $\mu = 0.25$, $k = 0.1$, $\tau_* = p_* = 4\,\mathrm{kPa}$, $C = \sigma = 1$, $\rho = \rho_0 = 300\,\mathrm{kg\,m^{-3}}$ are indicated.

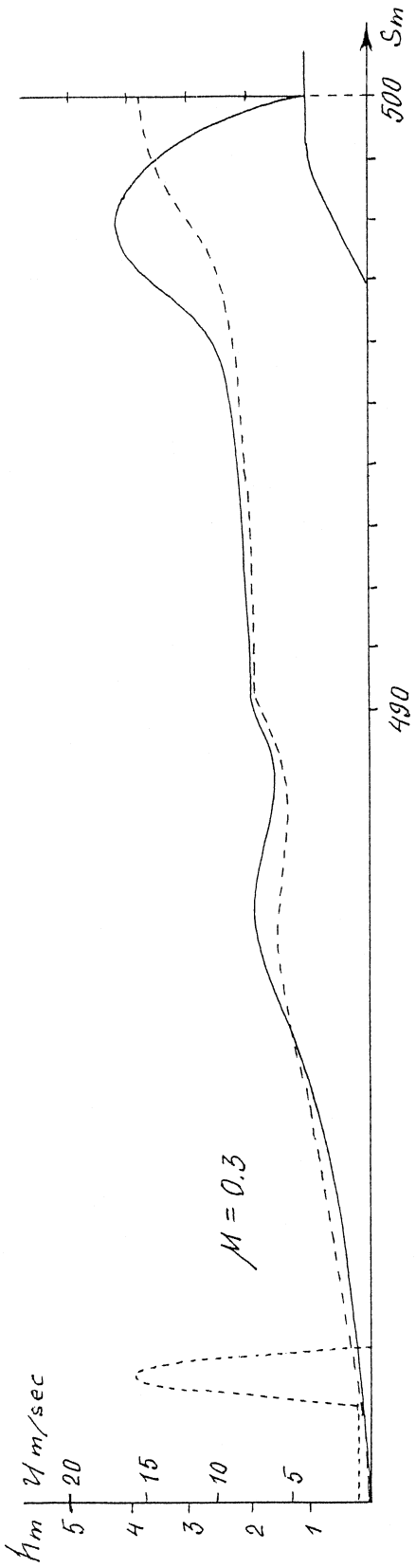

Figure S2.14: Numerical results from simulations with the full model. Note the change of horizontal scale at $S = 490\,\mathrm{m}$. The parameters are that of the standard set, except for $\mu = 0.3$ instead of 0.25 and a non-rectangular initial snow distribution (dotted line).